









RESEARCH ARTICLE | MARCH 01 2022

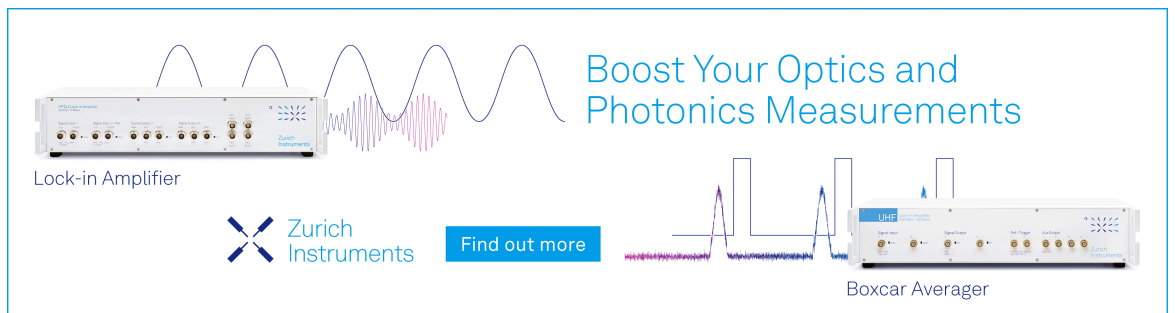
# High-precision background correction and artifact suppression for ultrafast spectroscopy by quasi-simultaneous measurements in a split-sample cell

E. Deniz ; J. G. Löffler ; A. Kondratiev ; A. R. Thun ; Y. Shen ; G. Wille ; J. Bredenbeck  



Rev. Sci. Instrum. 93, 033001 (2022)

<https://doi.org/10.1063/5.0079958>



Boost Your Optics and Photonics Measurements

Lock-in Amplifier

Zurich Instruments

Find out more

Boxcar Averager

# High-precision background correction and artifact suppression for ultrafast spectroscopy by quasi-simultaneous measurements in a split-sample cell

Cite as: *Rev. Sci. Instrum.* **93**, 033001 (2022); doi: [10.1063/5.0079958](https://doi.org/10.1063/5.0079958)

Submitted: 26 November 2021 • Accepted: 3 February 2022 •

Published Online: 1 March 2022



View Online



Export Citation



CrossMark

E. Deniz,  J. G. Löffler,  A. Kondratiev,  A. R. Thun,  Y. Shen,  G. Wille,  and J. Bredenbeck<sup>a)</sup> 

## AFFILIATIONS

Institute of Biophysics, Goethe University Frankfurt am Main, Frankfurt am Main 60438, Germany

<sup>a)</sup> Author to whom correspondence should be addressed: [bredenbeck@biophysik.uni-frankfurt.de](mailto:bredenbeck@biophysik.uni-frankfurt.de)

## ABSTRACT

Alternating acquisition of background and sample spectra is often employed in conventional Fourier-transform infrared spectroscopy or ultraviolet–visible spectroscopy for accurate background subtraction. For example, for solvent background correction, typically a spectrum of a cuvette with solvent is measured and subtracted from a spectrum of a cuvette with solvent and solute. Ultrafast spectroscopies, though, come with many peculiarities that make the collection of well-matched, subtractable background and sample spectra challenging. Here, we present a demountable split-sample cell in combination with a modified Lissajous scanner to overcome these challenges. It allows for quasi-simultaneous measurements of background and sample spectra, mitigating the effects of drifts of the setup and maintaining the beam and sample geometry when swapping between background and sample measurements. The cell is moving between subsequent laser shots to refresh the excited sample volume. With less than 45  $\mu\text{l}$  of solution for 150  $\mu\text{m}$  optical thickness, sample usage is economical. Cell assembly is a key step and covered in an illustrated protocol.

© 2022 Author(s). All article content, except where otherwise noted, is licensed under a Creative Commons Attribution (CC BY) license (<http://creativecommons.org/licenses/by/4.0/>). <https://doi.org/10.1063/5.0079958>

## I. INTRODUCTION

Subtracting backgrounds and artifacts is a recurring challenge in optical spectroscopy. A frequent case is the subtraction of solvent contributions from a sample's absorption in infrared (IR) or ultraviolet–visible (UV/VIS) transmission spectroscopy. For example, in conventional Fourier-transform (FT) IR spectroscopy,<sup>1</sup> this is usually achieved in sufficient quality by subtracting a solvent background spectrum from a separately measured spectrum of the sample containing solute and solvent.

In dispersive, pump–probe, or multipulse time-resolved IR spectroscopy, however, where spectra are quite sensitive to laser performance and setup alignment, subtraction of subsequent measurements typically gives only poor results caused by drifts during data acquisition due to changes in laser power and beam-pointing, as well as thermal lensing effects, combined with spatial inhomogeneities of

the detector. These effects aggravate with longer measurement times, which are required to reach a certain noise level.

To reduce the effects of drifts of experimental parameters, quasi-simultaneous interleaved measurements of background and sample spectra can be carried out. To this end, a sample cell and a background cell are alternately moved into and out of the beam. For an application in sensitive experiments, however, the miniscule differences in the geometry of two separate demountable cells (slightly wedged front and/or back windows in different orientations, difference in the angle of the sample with respect to the beam, and difference of the position in the direction of light propagation)—even with matching path length—are an obstacle to overcome in order to make the subtraction of quasi-simultaneous measurements work.

Flow cells are an option since they allow changing samples without disturbing the cell geometry or the setup alignment.<sup>2</sup> Bloem *et al.* used a flow cell with an automated syringe pump system to

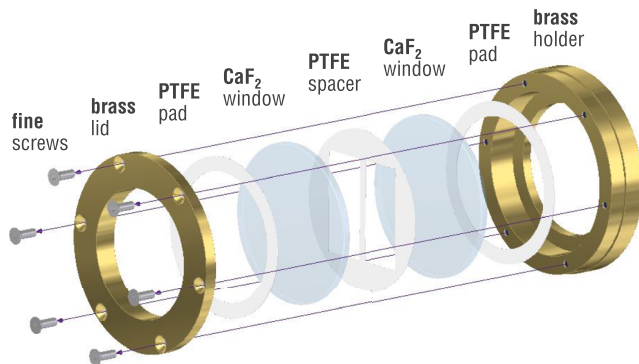


**FIG. 1.** Exploded view drawing of the split-sample cell. The holder is designed for 1.5 in.  $\text{CaF}_2$  windows, but a 1 in. version is also available and was also successfully tested. We can provide technical drawings of the split-sample cell upon request. The shown model has been generated using Solid Edge ST9 Software from Siemens.

swap the sample and background solutions in a femtosecond two-dimensional (2D) IR experiment.<sup>3</sup> Many time-resolved experiments, however, require a rapid exchange of the sample between subsequent laser shots, which is not easily achieved with the flow cell approach when the flow cell is at the same time used to swap between the sample and the background—unless large amounts of sample can be used. In addition, cross-contamination of the background solution and the sample solution must be avoided.

In many cases, the requirement of large amounts of sample is prohibitive, for example, in many studies of biomolecular systems.<sup>4–7</sup> For a broader application of quasi-simultaneous difference measurements in laser-based spectroscopy, an alternative approach for perturbation-free swapping of the background solution and the sample solution is necessary.

Here, we present a split-sample cell approach based on a common demountable measurement cell (see Fig. 1) and a Lissajous scanner. The advantage of a split-sample cell over using two separate cells is that it is much easier to maintain the geometry at the sample position because the beam is still passing the same optics [in this case, the calcium fluoride ( $\text{CaF}_2$ ) windows of the cell] when moving back and forth between the sample and the background compartment. The cell was designed with a particular focus on transient ultrafast VIS-pump-IR-probe measurements of proteins, but its features are interesting for a broad range of laser spectroscopic applications. Required modifications to already existing setups are minimal and affordable.

The idea is simple: (1) Divide the available volume of one cell into two compartments and load them with the background and sample solutions, respectively; (2) shuttle between the background and sample compartments between scans; and (3) subtract.

The first step is the key and rather delicate. Here, we provide a step-by-step protocol for a robust and routine cell assembly, tips and tricks for operating the split-sample cell, and demonstrations of high-precision background subtraction in a VIS-pump-IR-probe experiment that investigates vibrational energy transfer (VET) in a protein (PDZ3 of the postsynaptic density protein 95).<sup>8</sup> The system features a vibrational energy donor (azulenylalanine, AzAla)

excited at 613 nm and a vibrational energy sensor (azidohomoalanine, Aha) probed at  $2100\text{ cm}^{-1}$ .<sup>9</sup> The experiment is challenging because small absorption changes of a few  $\mu\text{OD}$  have to be measured in the presence of a 100-fold larger water background and sample heating.

## II. DESIGN OF THE SPLIT-SAMPLE CELL

### A. Components and assembly

The featured split-sample cell (see Fig. 1) is mounted in a Lissajous scanner, which continuously moves the sample so that subsequent laser shots interact with a different sample volume. The rotating motions of two motors (Trident Engineering DN22M-24+GPP22.0014) are translated on a vertical and a horizontal linear stage. The simultaneous harmonic motion along these stages at a given frequency ratio leads to a movement of the sample cell in a Lissajous pattern. Over time, the laser shots are thus distributed over a rectangular scan area [see Fig. 2(a)].

The Lissajous scanner also includes three manually adjustable linear stages for the spatial directions  $x$ ,  $y$ , and  $z$  with the  $z$ -stage

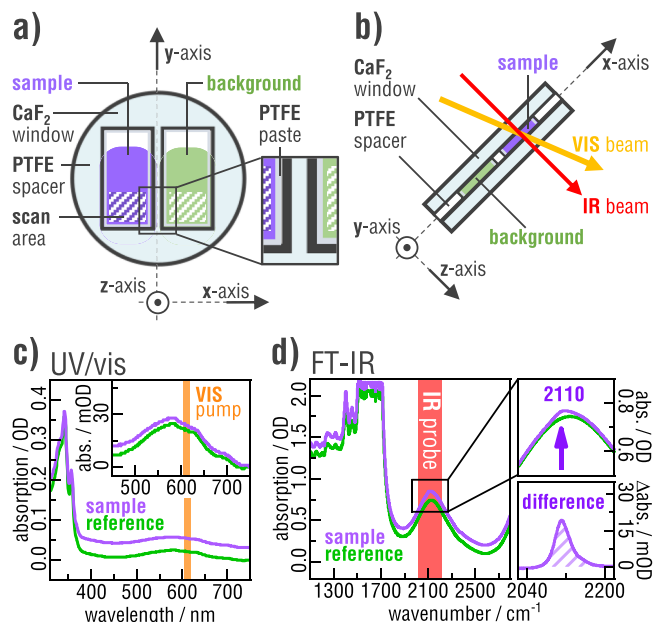


**FIG. 2.** Schematic drawing of the loaded split-sample cell and spectral properties of the sample and background solutions. (a) (Front view) The interface between the sample, spacer, and background solution has been zoomed in to highlight the PTFE paste sealing. (b) (Top view) The sample plane is aligned along the  $x$  axis, which is the single degree of freedom of the linear actuator switching back and forth between the sample and the background. (c) UV/VIS spectra of the sample and background solutions. An arbitrary offset has been introduced to show the almost congruent spectra. The inset zooms into the broad absorption band around 600 nm corresponding to the  $S_0 \rightarrow S_1$  transition. No offset has been introduced here, revealing the desired UV/VIS spectral similarity of the sample and the background. (d) FT-IR spectra of the sample and the background. An arbitrary offset has been introduced to show the otherwise almost congruent spectra. The tip of the broad water absorption band has been zoomed in with no offset, revealing the Aha band that is only present in the sample spectrum. It can be isolated by subtracting the background spectrum.

being parallel to the probe beam and the x- and y-stages spanning a plane parallel to the focal plane. These stages allow the positioning of the thin sample film within the focal plane of the IR beam. The x- and y-stages essentially provide an offset to the initial beam positions. We equipped the x-stage with an additional computer-controlled motor (MKS Newport, LTA-HL) to switch back and forth between two desired scan areas, i.e., the two compartments [see Fig. 2(a)] of the split-sample cell.

For the split-sample cell (see Fig. 1), we use two 1.5 in. CaF<sub>2</sub> windows of 2 mm thickness (Crystal GmbH). This gives enough space for two separate compartments with an area of 10 × 25 mm<sup>2</sup> each and a Lissajous scanning window of 7 × 6 mm<sup>2</sup> [see Fig. 2(a)]. The spacer creating the two compartments is cut from a polytetrafluoroethylene (PTFE) foil (Goodfellow Ltd.) with the required thickness (here 150 μm). The assembly of both windows with the spacer and solutions in between is placed in a custom-made brass holder and gently tightened with fine threads.

### B. Sample loading

While the design of the split-sample cell is straightforward, the sample loading is a rather delicate step and needs thorough preparations to avoid leakage or liquid exchange between the compartments. Note that the split-sample cell is, in principle, compatible with other solvents besides water [e.g., dimethyl sulfoxide (DMSO)] as long as they do not evaporate rapidly, which would make sample loading a challenging endeavor. For a detailed and illustrated step-by-step protocol for the assembly and loading process, see the [supplementary material](#). A brief description of the step-by-step protocol is described as follows: (1) Use a freshly cleaned and dried spacer. (2) Cover both sides of the spacer with a generous layer of PTFE paste (Carl Roth GmbH, art. nr. 124, consisting solely of polytetrafluoroethylene and perfluoropolyether). (3) Place the spacer onto the first CaF<sub>2</sub> window and make sure it is sticking everywhere. Pay particular attention to the thin bridge separating both compartments. (4) With a plastic pipette tip, gently and carefully apply PTFE paste around the inner edges of the compartments, eventually creating a PTFE sealing. (5) Pipette the sample and background solutions onto the lower edges of the respective compartments. (6) Carefully place the second window on the top, with first touching both droplets with the top window and then pressing them flat. (7) Tighten the fine screws in a crosswise fashion to avoid asymmetric tension. The solutions should evenly distribute in their respective compartments.

### C. Operation

It is crucial that the sample plane is aligned parallel to the translation axes of the linear actuators [see Fig. 2(b)]. Otherwise, the two compartments will end up at slightly different z-positions when moved into the beam, and focusing into the sample and beam overlap would differ for the two compartments. Note, the more similar the beam configuration for both scanning areas, the more similar are background signal intensities and thermal lensing effects, ensuring an accurate background and artifact suppression.

In the interleaved measurement of the sample and background spectra, compartments need to be switched either between single pump-probe delays or between whole scans (i.e., the complete series of delays). The former option provides a closer correlation between

the sample and background measurements, but it is also more time-consuming because switching between compartments takes 15 s with our current actuator. Therefore, we use the latter option in our measurements, still yielding highly satisfactory results in control experiments with identical samples in both compartments [see Fig. 3(c)].

## III. MATERIALS AND METHODS

### A. Sample preparation

For a detailed description of sample preparation, including protein expression and purification, peptide synthesis, and concentration determination, see the [supplementary material](#). A brief description of sample preparation is described as follows:

PDZ Aha mutants were concentrated to ~12 mM in aqueous buffer. The ligand was dissolved in the same buffer to a concentration of ~60 mM. Protein and ligand stock solutions were mixed to yield a protein/ligand complex concentration of at least 10 mM as determined via UV/VIS absorption of AzAla in the bound ligand at 341 nm with  $\epsilon_{341} = 4200 \text{ M}^{-1} \text{ cm}^{-1}$  [see Fig. 2(c)]. FT-IR spectra were recorded in the same cuvette as the UV/VIS spectra with 60 μm path length to check for the azide absorption at 2110 cm<sup>-1</sup> [see Fig. 2(d)], which was ~15 mOD, depending on the exact protein concentration, Aha labeling efficiency, and extinction coefficient. The azide absorption sits on a significant water background of ~0.75 OD, limiting the sample thickness in our laser measurements. Note that at the given protein concentration, the water absorption is decreased due to the displacement of water molecules. The optical density at the excitation wavelength was ~25 mOD, depending on the exact ligand concentration. Background samples with wild-type (wt) PDZ were prepared simultaneously and according to the same protocol, aiming for the same concentration.

Freshly prepared sample and background solutions were loaded into the split-sample cell with two compartments cut out of a PTFE spacer with 150 μm thickness. We loaded ~40 μl into a single compartment, which is ~15% less than the maximum capacity of the respective compartment to avoid overflowing and, thus, mixing of the sample and the background. For a detailed and illustrated description of split-sample cell loading, see the [supplementary material](#).

### B. Laser setup

A Ti:Sa regenerative amplifier system (Spitfire, Spectra-Physics) with 3 kHz repetition rate, generating 800 nm pulses with 100 fs pulse duration, and 1.6 mJ pulse energy pumped two optical parametric amplifiers (OPAs).

OPA I generated mid-IR probe pulses centered around 2110 cm<sup>-1</sup> via difference frequency generation in a silver thiogallate (AGS) crystal. The pulses were dispersed on a spectrometer (Triax, Jobin Yvon) with a 150 lines/mm grating and detected on a 2 × 64 pixels mercury-cadmium-telluride (MCT) detector (InfraRed Associates) cooled with an automated liquid nitrogen refilling system.<sup>10</sup>

OPA II generated 613 nm pump pulses via second harmonic generation of the signal beam in a β-barium-borate (BBO) crystal. The pump pulse energy was 18 μJ. A chopper blocked every

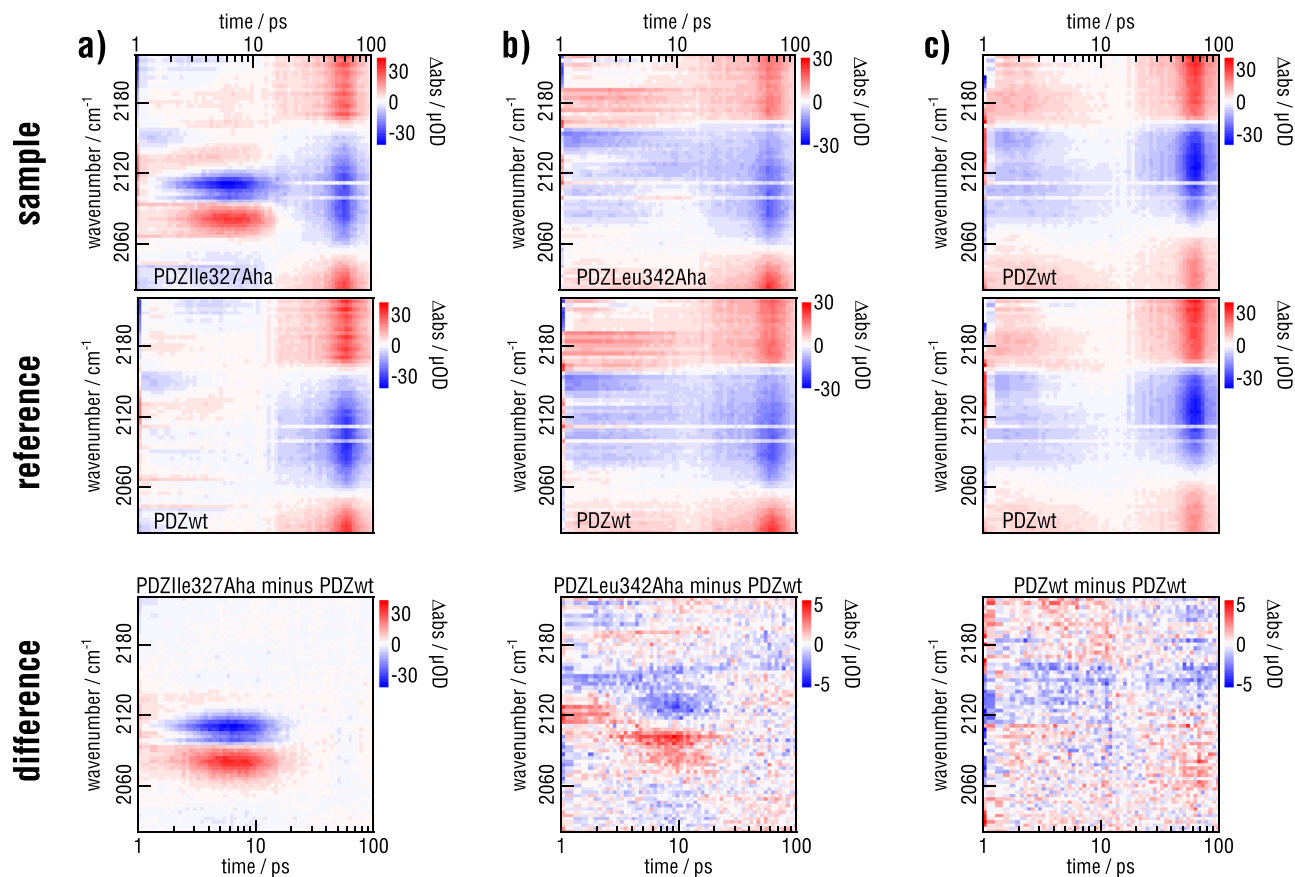


**FIG. 3.** TRIR spectra of PDZ variants before and after suppression of photothermal artifacts. (a) (Left column) TRIR spectra of PDZ Ile327Aha as a sample and PDZ wt as a background result in a tidy TRIR difference spectrum with a strong VET-signature of the Aha in PDZ at position 327. (b) (Middle column) TRIR spectra of PDZ Leu342Aha as a sample and PDZ wt as a background result in a tidy TRIR difference spectrum with a clear VET-signature of the Aha in PDZ at position 342 despite the extremely low signal amplitude of 5  $\mu\text{OD}$ . (c) (Right column) TRIR spectra of PDZ wt as a sample and as a background result in a flat TRIR difference spectrum with a remarkably low noise level of 2  $\mu\text{OD}$ . Note the different color scale in the two panels on the lower right.

other pulse, resulting in pump-on minus pump-off difference spectra. The polarization between the pump and the probe was set to the magic angle. The focal beam diameters were 100 and 80  $\mu\text{m}$  (full width at half maximum) for the pump and the probe, respectively.

### C. Transient IR spectroscopy

Transient IR (TRIR) spectra are difference spectra and were recorded with the featured split-sample cell in the following manner: First, pump-on minus pump-off difference spectra of the sample compartment are acquired at  $\sim 70$  different pump-probe delay times covering  $-40$  to 120 ps. After the scan, the pump light is blocked by a shutter to avoid unnecessary exposure, and the split-sample cell is moved to the background compartment to reproduce the measurement. One cycle of sample and background scan takes  $\sim 30$  min on our current setup: 15 min per compartment for  $\sim 70$  time points with 30 000 acquired laser shots per time point. For the noise level shown in Fig. 3, this cycle is repeated  $\sim 80$  times requiring in total about 40 h of continuous measurement time. Afterward, the data are averaged.

Once averaged for the sample and background compartments independently, the spectrum at  $-40$  ps is subtracted from all other time points to correct for contributions from the previous pump pulse. Afterward, we eliminate the big (600–800  $\mu\text{OD}$ , SFig. 2) and broad water response by subtracting the spectrum at 120 ps, which contains *only* the water signal, in a scaled fashion together with a time-dependent offset from all other time points. The two parameters are obtained by a best fit (see the [supplementary material](#) for a detailed description of the water background treatment). In a final step, unwanted features from the coherent artifact at early times and unpredictable signal changes over the whole TRIR spectrum are suppressed by subtracting the processed TRIR spectrum of the background compartment.

## IV. RESULTS AND DISCUSSION

To exemplify the performance of the split-sample cell, we present the VET-signal of an azide moiety incorporated in the form of Aha into the PDZ protein.<sup>8</sup> Pumping the azulene

moiety in the bound ligand with 613 nm light dumps vibrational energy into the protein–ligand complex within a split picosecond. The azide of Aha in PDZ responds to increasing vibrational energy by red shifting its stretching frequency. This is caused by anharmonic coupling to low-frequency modes receiving the vibrational energy.<sup>11–13</sup> In the transient spectrum, this results in the characteristic azide signature of positive (red) and negative (blue) features representing induced and reduced absorption, respectively.

Although the probed spectral window of the azide stretching frequency centered around  $2120\text{ cm}^{-1}$  is free from any other protein signals, the broad water absorption contributes a huge difference signal of  $600\text{--}800\ \mu\text{OD}$  (see SFig. 2). Despite our efforts for optimal alignment of the cell and the translation of the cell by the Lissajous scanner, as well as for as similar as possible the composition of the sample and background solutions, the water signals are not equal enough to subtract them to the required level of about  $2\ \mu\text{OD}$  (see the bottom row of Fig. 3). Therefore, a water correction is applied separately to the sample and background spectra, as detailed in Sec. III and the [supplementary material](#), before the sample and background spectra are subtracted.

The VET-response of water is almost two orders of magnitude stronger than the expected VET-response of the azide (see SFig. 2). The top row of Fig. 3 shows the already water signal subtracted TRIR spectra of three PDZ variants, i.e., two Aha-labeled mutants and one wild-type without the VET-sensor. All three TRIR spectra display a similar stripe pattern of absorption changes along the time axis with changes of sign along the wavenumber axis. Note that this pattern also occurs with the wild-type as a sample, that is, PDZ without any Aha as a VET-sensor, where one would expect the water signal subtraction to yield a flat baseline.

Details of the stripe pattern change from experiment to experiment even when the same sample is measured repeatedly after removing and inserting the sample cell and optimizing pump overlap again. Evidently, beam configuration, such as focusing, beam pointing, and pump–probe overlap, play a role. The change-of-sign of the stripe pattern coincides approximately with the four 16 pixel subarrays of the 64 pixel MCT detector. From those observations, we conclude that these patterns mainly arise from a heterogeneous response of the detector subarrays to beam pointing changes. They are induced by photothermal deflection of the probe beam due to thermal lensing induced within the sample upon pump pulse absorption.

In PDZ 327, the VET-response of Aha is large enough to emerge from the obscuring layer of thermal lensing artifacts. Although the noise level of  $<2\ \mu\text{OD}$  is remarkably low, the detection limit for VET-signals is determined by those photothermal artifacts, which are an order of magnitude higher. In PDZ 342, with a twice as large VET-pair distance compared to PDZ 327, it is hence not surprising that the anticipated weak VET-signal is disappearing under the artifacts. In fact, the PDZ 342 spectrum and the spectrum of the wild-type, i.e., with *no* expected VET-signal, look almost identical [see Figs. 3(b) and 3(c)].

The striking similarity of the patterns in the background in consecutive experiments inspired us to reproduce and subtract them in a quasi-simultaneous background measurement with the split-sample approach. The background solution contains the same components in matching concentrations except for the IR sensor amino acid.

With carefully adjusted concentrations and identical experimental conditions, TRIR spectra of both the sample and background solutions loaded into the split-sample cell reveal identical photothermal artifacts, which is the prerequisite for the subtraction step afterward.

Subtracting the background spectrum with the accurately reproduced thermal lensing artifacts isolates the VET-signal in PDZ 327. The photothermal background suppression uncovered even the drowned-out VET-response in PDZ 342, revealing the clearly recognizable VET-signature of the azide despite the small amplitude of only  $5\ \mu\text{OD}$ . Now, with the additional subtraction step, the lower level for signal detection is solely limited by the accuracy of the subtraction. The demo measurement of wild-type vs wild-type illustrates how precisely the thermal lensing artifacts can be reproduced over the whole TRIR spectrum. The difference spectrum displays just noise along both wavenumber and the time axis but no remnants of the stripe pattern. Considering a signal-to-noise ratio of at least 2:1, the achieved noise level of about  $2\ \mu\text{OD}$  allows assigning absorption changes with amplitudes as small as  $4\ \mu\text{OD}$  as actual signals in the presence of an  $800\ \mu\text{OD}$  water background.

## V. CONCLUSION

In summary, we established a combination of a Lissajous scanner and a split-sample cell, enabling various sorts of next-level difference spectroscopies. With the additional step of differencing, pump–probe techniques characterized by small signals sitting on a huge background reach higher contrast and sensitivity. Light-induced heating of samples and all concomitant side effects, such as difference signals of the solvent and thermal lensing artifacts, are precisely reproduced by a quasi-simultaneous background measurement for a high accuracy background subtraction.

The ability to measure two different samples at the same time opens the door for delicate applications, such as substrate- or ligand-induced 2D-IR difference spectroscopy.<sup>14</sup> Detecting absorption changes in a single digit  $\mu\text{OD}$  regime will resolve slightest band shifts related to miniscule structural changes in the surrounding of the observed oscillator.

## SUPPLEMENTARY MATERIAL

See the [supplementary material](#) for details on sample preparation, an illustrated cell assembly and loading protocol, and laser data postprocessing.

## ACKNOWLEDGMENTS

We acknowledge financial support from DFG (Grant Nos. BR 3746/4-1 and INST 161/722-1). E.D. acknowledges the Stiftung Polytechnische Gesellschaft for a MainCampus-doctus fellowship.

## AUTHOR DECLARATIONS

### Conflict of Interest

The authors have no conflicts to disclose.

## Author Contributions

E.D. designed the device and wrote the manuscript. J.G.L. wrote the scripts for data analysis. A.K., A.R.T., and G.W. wrote the data acquisition software and programmed the quasi-simultaneous measurement routine. E.D. and Y.S. established the cell assembly and loading protocol. J.B. planned and supervised research and revised the manuscript. E.D. and J.G.L. jointly performed experiments and analyzed the data. E.D. and J.G.L. contributed equally to this work.

## DATA AVAILABILITY

The data that support the findings of this study are available from the corresponding author upon reasonable request.

## REFERENCES

- <sup>1</sup>V. A. Lorenz-Fonfria, *Chem. Rev.* **120**, 3466 (2020).
- <sup>2</sup>J. Bredenbeck and P. Hamm, *Rev. Sci. Instrum.* **74**, 3188 (2003).
- <sup>3</sup>R. Bloem, K. Koziol, S. A. Waldauer, B. Buchli, R. Walser, B. Samatanga, I. Jelesarov, and P. Hamm, *J. Phys. Chem. B* **116**, 13705 (2012).
- <sup>4</sup>E. Deniz, L. Valiño-Borau, J. G. Löffler, K. B. Eberl, A. Gulzar, S. Wolf, P. M. Durkin, R. Kaml, N. Budisa, G. Stock, and J. Bredenbeck, *Nat. Commun.* **12**, 3284 (2021).
- <sup>5</sup>C. R. Hall, J. Tolentino Collado, J. N. Iuliano, K. Adamczyk, A. Lukacs, G. M. Greetham, I. V. Sazanovich, P. J. Tonge, and S. R. Meech, *J. Phys. Chem. B* **123**(45), 9592–9597 (2019).
- <sup>6</sup>T. Stensitzki, S. Adam, R. Schlesinger, I. Schapiro, and K. Heyne, *Molecules* **25**, 848 (2020).
- <sup>7</sup>M. Asido, P. Eberhardt, C. N. Kriebel, M. Braun, C. Glaubitz, and J. Wachtveitl, *Phys. Chem. Chem. Phys.* **21**, 4461 (2019).
- <sup>8</sup>T. Baumann, M. Hauf, F. Schildhauer, K. B. Eberl, P. M. Durkin, E. Deniz, J. G. Löffler, C. G. Acevedo-Rocha, J. Jaric, B. M. Martins, H. Dobbek, J. Bredenbeck, and N. Budisa, *Angew. Chem., Int. Ed.* **58**, 2899 (2019).
- <sup>9</sup>H. M. Müller-Werkmeister and J. Bredenbeck, *Phys. Chem. Chem. Phys.* **16**, 3261 (2014).
- <sup>10</sup>E. Deniz, K. B. Eberl, and J. Bredenbeck, *Rev. Sci. Instrum.* **89**, 116101 (2018).
- <sup>11</sup>D. V. Kurochkin, S. R. G. Naraharisetty, and I. V. Rubtsov, *Proc. Natl. Acad. Sci. U. S. A.* **104**, 14209 (2007).
- <sup>12</sup>I. V. Rubtsov, *Acc. Chem. Res.* **42**, 1385 (2009).
- <sup>13</sup>P. Hamm, S. M. Ohline, and W. Zinth, *J. Chem. Phys.* **106**, 519 (1997).
- <sup>14</sup>S. Hume, G. M. Greetham, P. M. Donaldson, M. Towrie, A. W. Parker, M. J. Baker, and N. T. Hunt, *Anal. Chem.* **92**, 3463 (2020).